Letter Vol. 48, No. 2 / 15 January 2023 / Optics Letters 493

Optics Letters

Nonlinearity measurement undergoing dispersion and loss

David Castelló-Lurbe,[1,2,3,*,†] Christian Cuadrado-Laborde,[4,†] Enrique Silvestre,[1,5] Antonio Díez,[1,2] and Miguel V. Andrés[1,2]

[1]Institut Universitari de Ciències dels Materials, Universitat de València, Catedrático Agustín Escardino 9, 46980 Paterna, Spain
[2]Departament de Física Aplicada i Electromagnetisme, Universitat de València, Dr. Moliner 50, 46100 Burjassot, Spain
[3]Brussels Photonics (B-PHOT), Department of Applied Physics and Photonics, Vrije Universiteit Brussel, Pleinlaan 2, 1050 Brussel, Belgium
[4]Instituto de Física Rosario (CONICET-UNR), Blvr. 27 de Febrero 210bis, S2000EZP Rosario, Argentina
[5]Departament d'Òptica i Optometria i Ciències de la Visió, Universitat de València, Dr. Moliner 50, 46100 Burjassot, Spain
*Corresponding author: david.castello-lurbe@uv.es
†These authors contributed equally to this work.

Received 18 November 2022; revised 13 December 2022; accepted 13 December 2022; posted 13 December 2022; published 11 January 2023

Accurate knowledge of the nonlinear coefficient is extremely important to make reliable predictions about optical pulses propagating along waveguides. Nevertheless, determining this parameter when dispersion and loss are as important as nonlinear effects brings both theoretical and experimental challenges that have not yet been solved. A general method for measuring the nonlinear coefficient of waveguides under these demanding conditions is here derived and demonstrated experimentally in a kilometer-long standard silica fiber pumped close to 2 μm.

© 2023 Optica Publishing Group under the terms of the Optica Open Access Publishing Agreement

https://doi.org/10.1364/OL.481445

Nonlinear optical phenomena in guiding media are generally studied based on the propagation of the envelopes of the electromagnetic field modes [1]. Consequently, the nonlinear dynamics of these systems depend on several modal parameters such as the nonlinear coefficient γ, the group-velocity dispersion β_2, or the linear loss α [1]. Their accurate measurement thus becomes essential in the nonlinear modeling of fibers or integrated waveguides. Although β_2 and α can be precisely determined at low powers [2], where nonlinearities can be safely neglected, γ values suffer from uncertainties of a fundamental nature due to dispersion or loss [3,4].

The traditional inaccuracies in γ caused by dispersive effects have recently been overcome in Ref. [4]. The key difference of this novel method with respect to previous techniques [5–8] is to rely on an exact conservation law of the nonlinear Schrödinger equation (NLSE) instead of solving it approximately, which releases the measurement of γ from any assumption beyond the NLSE itself. Furthermore, if this approach could be applied to more complex systems such as waveguides where the dispersion slope or the loss is significant, then the lack of exact solutions to generalized versions of the NLSE would not limit experimental γ accuracies. Including higher-order dispersion terms should not represent, in principle, a major constraint since the corresponding nonlinear models fulfill extensions of the conservation law [9]. In contrast, accounting for a loss comparable to dispersion and nonlinearities defies the very basis of this framework as the conservation law is then broken [4].

Despite these envisaged issues, strong interplays between nonlinearities, dispersion (or diffraction), and loss (or gain) may occur in several cases with fundamental and technological relevance including nonlinear plasmonics [10,11], nonlinear $\mathcal{PT}$-symmetric photonic systems [12], and nonlinear optics in integrated waveguides with 2D materials [13,14] or dispersive nonlinearities [15]. In addition, measurements of γ in lossy waveguides can be instrumental to check experimentally the different theoretical expressions reported to date for γ [16], as well as an effective means to study γ in active fibers. These current research topics call for sound solutions to the complexities inherent to determining γ when dispersion and loss are on an equal footing with nonlinear processes.

Here, an approach to determine β_2/γ, and hence γ if β_2 is available, in lossy waveguides is developed and proved numerically and experimentally using, in particular, a 1.16-km-long Corning SMF-28e+ fiber pumped at 1.951 μm, where it features a 10.9-dB km^{-1} loss.

Let us consider the generalized NLSE in a lossy waveguide,

$$\frac{\partial}{\partial z}A(z,T) = -\frac{\alpha}{2}A - i\frac{\beta_2}{2}\frac{\partial^2 A}{\partial T^2} + i\gamma|A(z,T)|^2 A, \tag{1}$$

where A is the complex envelope of the electric field and T denotes the time in the retarded frame [1]. Following Ref. [4], Eq. (1) implies

$$-\frac{\mathrm{d}}{\mathrm{d}z}\rho(z) - \alpha\rho(z) = \frac{\beta_2}{2\gamma}\frac{\mathrm{d}}{\mathrm{d}z}\mu_2(z), \tag{2}$$

where $\rho(z) = (1/2)\int_{-\infty}^{+\infty}|A|^4\,\mathrm{d}T / \int_{-\infty}^{+\infty}|A|^2\,\mathrm{d}T$ and $\mu_2(z) = \int_{-\infty}^{+\infty}\Omega^2|\tilde{A}|^2\,\mathrm{d}\Omega / \int_{-\infty}^{+\infty}|\tilde{A}|^2\,\mathrm{d}\Omega$, with $\tilde{A} = \tilde{A}(z,\Omega)$ being the Fourier transform of A and Ω the relative angular frequency. If Eq. (2) is

rewritten as

$$-e^{-\alpha z}\frac{\mathrm{d}}{\mathrm{d}z}\varrho(z)=\frac{\beta_2}{2\gamma}\frac{\mathrm{d}}{\mathrm{d}z}\mu_2(z), \tag{3}$$

where $\varrho(z)=e^{\alpha z}\rho(z)$, and it is integrated over a distance L where $\varrho(z)$ grows monotonically, then, according to the mean value theorem,

$$-e^{-\alpha\ell}\,\Delta\varrho=\frac{\beta_2}{2\gamma}\,\Delta\mu_2, \tag{4}$$

with $0<\ell<L$, where $\Delta\varrho=e^{\alpha L}\rho(L)-\rho(0)$ and $\Delta\mu_2=\mu_2(L)-\mu_2(0)$. Note that, in the lossless case, $e^{-\alpha\ell}\,\Delta\varrho=\rho(L)-\rho(0)=\Delta\rho$, and thus measuring input and output values of ρ and μ_2 at different powers suffices to determine β_2/γ, as reported in Ref. [4]. In the lossy case, however, and particularly when $\alpha L>1$, ℓ is required to obtain β_2/γ, as Eq. (4) shows. This fact reflects that information of ρ along the waveguide is needed here, as seen by integrating Eq. (2),

$$e^{-\alpha\ell}=\frac{\Delta\rho+\alpha\int_0^L\rho(z)\mathrm{d}z}{\Delta\varrho}. \tag{5}$$

Although the magnitudes ρ and μ_2 are used in this work for experimental purposes, they turn to be very convenient to study the NLSE analytically. In this regard, a key step forward has been done in Ref. [17], where dynamical equations for $\rho(z)$ and $\mu_2(z)$ have been derived in the lossless case. Interestingly, if loss were incorporated into this theory, then ℓ, and hence β_2/γ, could be determined. This derivation has been carried out in Appendix A and results in the following propagation equation for $f(z)=(\varrho(z)/\varrho(0))^{-1}$ even in the presence of high loss,

$$f^3\frac{\mathrm{d}^2f}{\mathrm{d}z^2}=32\,\kappa^2\,\beta_2^2\,\mu_{20}^2\left(\frac{\gamma}{\beta_2}\frac{\rho_0}{\mu_{20}}e^{-\alpha z}f+1\right), \tag{6}$$

where $\rho_0=\rho(0)$, $\mu_{20}=\mu_2(0)$, and κ is a shape factor defined in Ref. [17]. Note that Eq. (6) decouples the evolution of $\rho(z)$ from $\mu_2(z)$ and thus it also represents significant progress with respect to Ref. [17]. In addition, setting input powers so that $\gamma\rho_0/(|\beta_2|\mu_{20})e^{-\alpha z}f\gg 1$ holds and thus the system does not enter the linear regime despite the loss, Eq. (6) can then be simplified to

$$f^2\frac{\mathrm{d}^2f}{\mathrm{d}z^2}=\mathrm{sign}(\beta_2)\,\eta^2\,\rho_0\,\mu_{20}\,e^{-\alpha z}, \tag{7}$$

where $\eta^2=32\,\kappa^2\,|\beta_2|\,\gamma$. It is worth remarking that the initial conditions enter Eq. (7) via $\rho_0\,\mu_{20}$ and, attending to Eq. (4), $\mathrm{sign}(\beta_2)=\mathrm{sign}(-\Delta\varrho/\Delta\mu_2)$ can be directly obtained.

Now let us discuss how Eq. (7) enables the measurement of β_2/γ via Eq. (4). For each pair of values ρ_0 and μ_{20}, η^2 can be fitted so that Eq. (7) recovers the corresponding experimental output value $f(L)$. Subsequently, $e^{-\alpha\ell}$ (for the ρ_0 and μ_{20} under consideration) can be evaluated by means of Eq. (7) and Eq. (5). Then, β_2/γ, and thus γ if β_2 is available, can be derived using Eq. (4). Finally, such a γ value can serve as a seed to initiate an iterative procedure to evaluate $e^{-\alpha\ell}$ directly via Eq. (1), and hence γ through Eq. (4), to a greater accuracy until convergence is reached. In the next paragraph, this method is illustrated and tested numerically using parameters values corresponding to an SMF28 fiber pumped at 1.951 μm, which is the fiber eventually employed in our proof-of-concept experiment.

Let us consider 90-ps-long sech pulses propagating 1.16 km along a fiber with $\alpha=2.5\times10^{-3}\,\mathrm{m}^{-1}$, $\beta_2=-75\,\mathrm{ps}^2\,\mathrm{km}^{-1}$ and $\gamma=0.68\,\mathrm{W}^{-1}\,\mathrm{km}^{-1}$. Note that $\alpha L\sim 3$, which is approximately

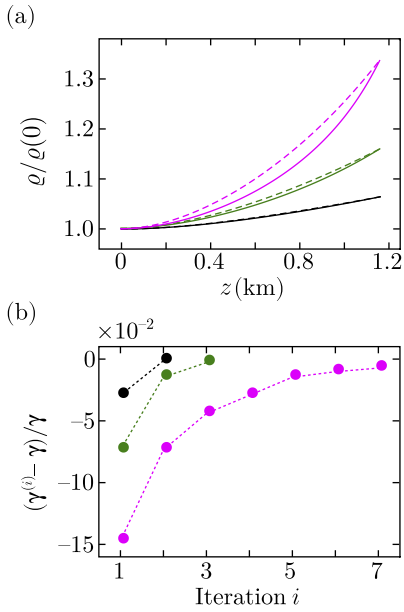

Fig. 1. (a) Comparison between the results given by Eq. (1) (solid lines) and Eq. (7) (dashed lines) for 10 W (black curves), 20 W (green curves), and 30 W (pink curves) of peak power. (b) Convergence study to determine γ in the cases in panel (a).

two orders of magnitude larger than in Ref. [4]. It is worth emphasizing that our approach is not circumscribed to sech pulses pumped in the anomalous dispersion regime, but these conditions will correspond to our experiment specifically. For pulse peak powers of 10 W, 20 W, and 30 W, the evolution of $\varrho(z)/\varrho(0)$ predicted by Eqs. (1) and (7) (with η^2 values selected to match the output values, as explained in the previous paragraph) are compared in Fig. 1(a). Based on the results provided by Eq. (7), $e^{-\alpha\ell}$ is found to be 0.222 for 10 W, 0.213 for 20 W, and 0.198 for 30 W. These correction factors due to loss allow a first approximation to γ given by $\gamma^{(1)}=0.66\,\mathrm{W}^{-1}\,\mathrm{km}^{-1}$ for 10 W, $\gamma^{(1)}=0.63\,\mathrm{W}^{-1}\,\mathrm{km}^{-1}$ for 20 W, and $\gamma^{(1)}=0.58\,\mathrm{W}^{-1}\,\mathrm{km}^{-1}$ for 30 W from Eq. (4). Once seed values for γ are available, $e^{-\alpha\ell}$ can be directly evaluated, for each input peak power, through Eq. (1) to improve the measurement accuracy. The outcome of each iteration is plotted in Fig. 1(b), which also shows convergence to the real value, $\gamma=0.68\,\mathrm{W}^{-1}\,\mathrm{km}^{-1}$, after a few iterations. Higher input powers require more iterations because the estimate provided by Eq. (7) is more accurate at lower input powers, as can be seen in Fig. 1(a). These simulations support the feasibility of our approach and, as such, bring us to its experimental test.

For our proof-of-concept experiment, ~ 90-ps-long pulses delivered at 1.951 μm from a passively mode-locked polarization-maintaining (PM) thulium-doped fiber (TDF) with a repetition rate of 18.45 MHz are amplified in a PM TDF amplifier and launched to a 1.16-km-long Corning SMF28e+. The spectra, temporal waveforms, and optical powers were recorded at both the input and output of the optical fiber under test for different input powers. For this purpose, an optical spectrum analyzer (50-pm resolution) and a digital sampling oscilloscope (20-GHz bandwidth) in conjunction with a 2-μm InGaAs photodetector (ET-5000F, Electro-Optics Technology, see Appendix B for more information) were used, as sketched in Fig. 2. A variable optical attenuator was also included to fix the operation of

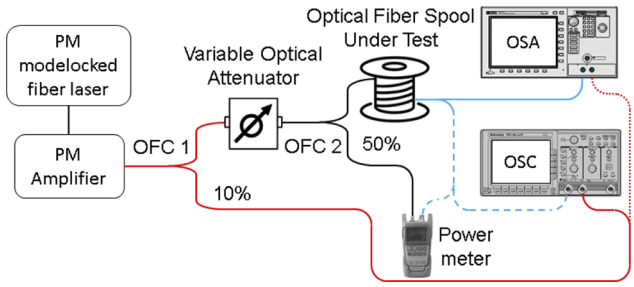

Fig. 2. Experimental setup, where OFC, optical fiber coupler; OSA, optical spectrum analyzer; OSC, oscilloscope; and the dashed/dotted lines mean consecutive (non-simultaneous) measurements.

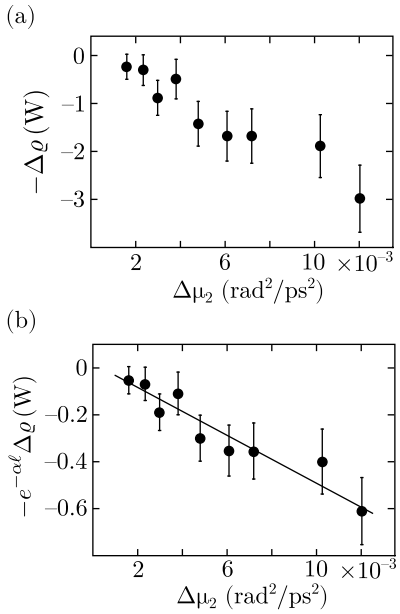

Fig. 3. (a) Raw results obtained directly from experimental data. (b) Processed results including correction factors due to loss (see details in the text).

the PM amplifier to a single point. Input mean powers between 27 mW and 72 mW were considered. The bare values measured in this experiment are shown in Fig. 3(a). Processing these data following the steps outlined above (and considering a 6% error due to the precision of power measurements in the ρ values), $\beta_2/\gamma = -102 \pm 13\,\mathrm{ps^2\,W}$ is derived from Fig. 3(b).

To check our result, on the one hand, $\beta_2 = -75 \pm 4\,\mathrm{ps^2\,km^{-1}}$ was measured using an optical-fiber version of a standard interferometric technique [2]. On the other hand, the value of γ measured at 1550 nm using our method for low-loss fibers [4] was scaled according to our numerical simulations (which were in line with Ref. [18]) and obtained $\gamma = 0.68 \pm 0.06\,\mathrm{W^{-1}\,km^{-1}}$. Consequently, $\beta_2/\gamma = -110 \pm 6\,\mathrm{ps^2\,km^{-1}}$, which is compatible with our direct measurement and validates our approach experimentally. Taking into account the error margins of this proof-of-concept experiment, no further iterations were carried out.

Finally, it is worth pointing out error sources that do not intrinsically limit our approach, but are related to the specific conditions of the setup where this measurement has been carried out. Having employed ~ 90-ps-long pulses, relatively small $\Delta\varrho$ are produced so that ϱ uncertainties become more relevant when measuring β_2/γ. Moreover, under anomalous dispersion, such long pulses can be more sensitive to instabilities if too high powers are employed [1].

In conclusion, a successful measurement of β_2/γ, and hence γ if β_2 is available, has been demonstrated in guiding media where nonlinearities, dispersion, and loss play an equally important role. Our approach is built upon the extension of a conservation law of the NLSE to lossy waveguides. As such, this method can be very useful in current areas of nonlinear optics exploiting plasmons, $\mathcal{PT}$-symmetry, 2D materials, or dispersive nonlinearities, even to discriminate competing nonlinear theories.

APPENDIX A: NONLINEAR PROPAGATION EQUATION FOR ϱ

The derivation of Eq. (6) is outlined in this section. On the one hand, the dynamical equation for the inverse generalized dispersive length, $\mathcal{L}_\mathrm{D}^{-1}(z) = (\beta_2/2)\mu_2(z)$, is obtained including the exponential decay of the pulse energy along z in the procedure described in the appendix of Ref. [17]. This modification turns into

$$\frac{\mathrm{d}\mathcal{L}_\mathrm{D}^{-1}}{\mathrm{d}z} = 8\,\kappa\,\mathrm{sign}(\beta_2)e^{\alpha z}\frac{L_\mathrm{NL}}{L_\mathrm{D}}(\mathcal{L}_\mathrm{NL}^{-1})^2 \times\left(4\,\mathrm{sign}(\beta_2)L_\mathrm{D}\mathcal{L}_\mathrm{D}^{-1} - 8\,e^{2\alpha z}L_\mathrm{NL}^2(\mathcal{L}_\mathrm{NL}^{-1})^2\right)^{1/2}, \tag{8}$$

where $\mathcal{L}_\mathrm{NL}^{-1}(z) = \gamma\rho(z)$ corresponds to the inverse generalized nonlinear length [4,9,17], and L_NL and L_D denote the classical nonlinear and dispersive length parameters, respectively [1].

Let us now define $\hat{\varrho}(z) = \varrho(z)/\varrho(0)$ and $\hat{\mu}_2(z) = \mu_2(z)/\mu_2(0)$, and rewrite Eqs. (3) and (8) as

$$\frac{\mathrm{d}\hat{\varrho}}{\mathrm{d}z} = -\frac{1}{2}\frac{\mu_{20}}{\rho_0}\frac{\beta_2}{\gamma}e^{\alpha z}\frac{\mathrm{d}\hat{\mu}_2}{\mathrm{d}z}, \tag{9}$$

$$\frac{\mathrm{d}\hat{\mu}_2}{\mathrm{d}z} = 8\sqrt{2}\,\kappa\,\gamma\,\rho_0\,e^{-\alpha z}\,\hat{\varrho}^2\,(\hat{\mu}_2 - \hat{\varrho}^2)^{1/2}, \tag{10}$$

respectively. Using Eq. (10), Eq. (9) implies

$$\left(\frac{1}{\hat{\varrho}^2}\frac{\mathrm{d}\hat{\varrho}}{\mathrm{d}z}\right)^2 = 32\,\kappa^2\beta_2^2\,\mu_{20}^2\,(\hat{\mu}_2 - \hat{\varrho}^2). \tag{11}$$

Finally, Eq. (6) is obtained deriving Eq. (11) and writing $\mathrm{d}\hat{\mu}_2/\mathrm{d}z$ in terms of $\mathrm{d}\hat{\varrho}/\mathrm{d}z$ employing Eq. (9), which decouples the propagation equation for $\hat{\varrho}$ from $\hat{\mu}_2$.

APPENDIX B: PHOTODETECTOR RESPONSE FUNCTION

Relying on second harmonic generation, autocorrelators typically require a power level that might not be reachable at the output in this context of high loss, and consequently ρ would have to be determined through direct photodetection. Indeed, this has been the case here. Attending to the intensity values below the offset observed in the oscillograms plotted in Fig. 4(a), photodetectors can distort the optical pulse shapes due to the so-called ringing when they are optimized for frequency-domain applications [19]. At first sight, this technical issue could severely hinder accurate measurements of $\Delta\varrho$ and, as such,

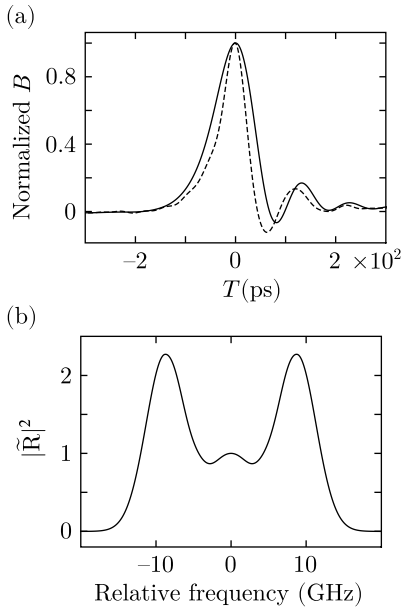

Fig. 4. (a) Normalized photodetected intensity profiles at the input (solid line) and output (dashed line). (b) Spectrum of the photodetector response function.

must be carefully analyzed. Let us express ρ in terms of the photodetector output $B(t) = \int_{-\infty}^{+\infty} R(\tau)|A(t-\tau)|^2\,\mathrm{d}\tau$,

$$\rho(z) = \frac{1}{4\pi}\frac{\displaystyle\int_{-\infty}^{+\infty} |\tilde{R}(\Omega)|^{-2}|\tilde{B}(z,\Omega)|^2\,\mathrm{d}\Omega}{\displaystyle\int_{-\infty}^{+\infty} B(z,t)\,\mathrm{d}t}, \tag{12}$$

where R is the response function of the photodetector satisfying $\int_{-\infty}^{+\infty} R(\tau)\,\mathrm{d}\tau = 1$. Based on Eq. (12), a precise measurement of ρ employing distorted pulses due to the photodetection is still possible provided the spectrum of the photodetector response function, $|\tilde{R}(\Omega)|^2$, is known. Accordingly, $|\tilde{R}(\Omega)|^2$ was also characterized experimentally, see Fig. 4(b), to process our data correctly.

Funding. Fonds Wetenschappelijk Onderzoek (147788/12ZN720N); European Commission (H2020-MSCA-RISE-2019-872049); Generalitat Valenciana (IDIFEDER/2020/064, PROMETEO/2019/048); European Regional Development Fund (PDI2019-104276RB-I00); Ministerio de Ciencia e Innovación (PDI2019-104276RB-I00); Ministerio de Universidades (María Zambrano fellowship ZA21-053, Next Generation EU).

Disclosures. The authors declare no conflicts of interest.

Data availability. Data underlying the results presented in this paper are not publicly available at this time but may be obtained from the authors upon reasonable request.

REFERENCES

1. G. P. Agrawal, *Nonlinear Fiber Optics* (Academic, 2013).
2. P. Hlubina, Opt. Commun. **193**, 1 (2001).
3. A. Lamminpää, T. Niemi, E. Ikonen, P. Marttila, and H. Ludvigsen, Opt. Fiber Technol. **11**, 278 (2005).
4. D. Castelló-Lurbe, A. Carrascosa, E. Silvestre, A. Díez, J. V. Erps, N. Vermeulen, and M. V. Andrés, Opt. Lett. **45**, 4432 (2020).
5. Y. Namihira, A. Miyata, and N. Tanahashi, Electronic Letters **30**, 1171 (1994).
6. A. Boskovic, S. V. Chernikov, J. R. Taylor, L. Gruner-Nielsen, and O. A. Levring, Opt. Lett. **21**, 1966 (1996).
7. J. Fatome, S. Pitois, and G. Millot, Opt. Fiber Technol. **12**, 243 (2006).
8. E. Rivera-Perez, A. Carrascosa, A. Díez, E. P. Alcusa-Sáez, and M. V. Andrés, Appl. Phys. Lett. **113**, 011108 (2018).
9. D. Castelló, P. Andrés, and E. Silvestre, Opt. Express **21**, 28550 (2013).
10. A. R. Davoyan, I. V. Shadrivov, and Y. S. Kivshar, Opt. Express **17**, 21732 (2009).
11. M. Kauranen and A. V. Zayats, Nat. Photonics **6**, 737 (2012).
12. S. V. Suchkov, A. A. Sukhorukov, J. Huang, S. V. Dmitriev, C. Lee, and Y. S. Kivshar, Laser Photonics Rev. **10**, 177 (2016).
13. Y. Wang, V. Pelgrin, S. Gyger, G. M. Uddin, X. Bai, C. Lafforgue, L. Vivien, K. D. Jöns, E. Cassan, and Z. Sun, ACS Photonics **8**, 2713 (2021).
14. Y. Zhang, J. Wu, Y. Yang, Y. Qu, H. E. Dirani, R. Crochemore, C. Sciancalepore, P. Demongodin, C. Grillet, C. Monat, B. Jian, and D. J. Moss, IEEE J. Sel. Top. Quantum Electron. **29**, 1 (2023).
15. D. Castelló-Lurbe, Opt. Lett. **47**, 1299 (2022).
16. G. H. Y. Li, A. Tuniz, and C. M. de Sterke, Opt. Lett. **45**, 5041 (2020).
17. D. Castelló-Lurbe, Opt. Lett. **46**, 4152 (2021).
18. M. Deroh, J. C. Beugnot, H. Maillotte, T. Sylvestre, K. Hammani, C. Finot, and B. Kibler, J. Opt. Soc. Am. B **37**, 3792 (2020).
19. https://www.newport.com/t/high-speed-detectors.